Proceedings of the ASME 2011 Internal Combustion Engine Division Fall Technical Conference
ICEF2011
October 2-5, 2011, Morgantown, West Virginia, USA

ICEF2011-60051

SIMULATING FLAME LIFT-OFF CHARACTERISTICS OF DIESEL AND BIODIESEL FUELS USING DETAILED CHEMICAL-KINETIC MECHANISMS AND LES TURBULENCE MODEL

Sibendu Som
Argonne National Laboratory
Argonne, IL 60439, USA

Douglas E. Longman
Argonne National Laboratory
Argonne, IL 60439, USA

Zhaoyu Luo
University of Connecticut
Storrs, CT 06269, USA

Max Plomer
University of Connecticut
Storrs, CT 06269, USA

Tianfeng Lu
University of Connecticut
Storrs, CT 06269, USA

Peter K. Senecal
Convergent Science, Inc.
Middleton, WI 53562, USA

Eric Pomraning
Convergent Science, Inc.
Middleton, WI 53562, USA

ABSTRACT

Combustion in direct-injection diesel engines occurs in a lifted, turbulent diffusion flame mode. Numerous studies indicate that the combustion and emissions in such engines are strongly influenced by the lifted flame characteristics, which are in turn determined by fuel and air mixing in the upstream region of the lifted flame, and consequently by the liquid breakup and spray development processes. From a numerical standpoint, these spray combustion processes depend heavily on the choice of underlying spray, combustion, and turbulence models. The present numerical study investigates the influence of different chemical kinetic mechanisms for diesel and biodiesel fuels, as well as Reynolds-averaged Navier-Stokes (RANS) and large eddy simulation (LES) turbulence models on predicting flame lift-off lengths (LOLs) and ignition delays. Specifically, two chemical kinetic mechanisms for n-heptane (NHPT) and three for biodiesel surrogates are investigated. In addition, the RNG k-ε (RANS) model is compared to the Smagorinsky based LES turbulence model. Using adaptive grid resolution, minimum grid sizes of 250 μm and 125 μm were obtained for the RANS and LES cases respectively. Validations of these models were performed against experimental data from Sandia National Laboratories in a constant volume combustion chamber. Ignition delay and flame lift-off validations were performed at different ambient temperature conditions. The LES model predicts lower ignition delays and qualitatively better flame structures compared to the RNG k-ε model. The use of realistic chemistry and a ternary surrogate mixture, which consists of methyl decanoate, methyl 9-decenoate, and NHPT, results in better predicted LOLs and ignition delays. For diesel fuel though, only marginal improvements are observed by using larger size mechanisms. However, these improved predictions come at a significant increase in computational cost.

1 INTRODUCTION

Fuel spray and combustion processes are extremely complex. They involve transient, two-phase turbulent flows, elevated pressures, and a wide range of temporal and spatial scales. Consequently, the experimental, theoretical, and computational studies of these flows have been challenging. The spray combustion processes in compression ignition engines are characterized by strong interactions between the liquid length and LOL [1,2,3,4]. The liquid length is defined as the farthest penetration of liquid fuel in terms of the axial

 Copyright © 2011 by ASME

location [5], and it is established where the total fuel evaporation rate equals the injection rate. It represents a global parameter for characterizing the atomization and vaporization behavior. The LOL is defined as the farthest upstream axial location of combustion, and it has been used to characterize the combustion behavior, since the LOL is largely determined by the fuel atomization, vaporization, subsequent fuel-air mixing, and air entrainment upstream of the liftoff location. These processes clearly play a critical role in determining the engine combustion and emission characteristics. For instance, correlation was observed between the soot distribution and LOL for diesel jets in the recent experiments by Pickett and Siebers [6,7].

In the past decade, several studies were performed by researchers at Sandia National Laboratories to provide high-fidelity measurements of parameters such as spray penetration, liquid length, vapor penetration, mixture-fraction [8,9,10], ignition delay, LOL, and soot emissions for a range of ambient and injection conditions, in a constant volume combustion vessel. A variety of fuels and fuel surrogates, such as diesel #2, biodiesel, NHPT and n-dodecane, were studied in these experiments, and the resulting dataset can be accessed through the Engine Combustion Network [11]. Only recently, this high-fidelity dataset has been used for spray combustion model development and validation.

One of the first studies to model the liquid length and flame LOL was performed by Senecal et al. using KIVA/SAGE with NHPT as the fuel surrogate [12]. The modeling approach involved the direct integration of complex chemistry in homogenous (perfectly mixed) computational cell. Liquid length, ignition delay, and LOL were well captured at different ambient and injection conditions. Kong et al. [13] also used NHPT as a surrogate for diesel fuel, and the reaction mechanism consists of 40 species and 165 reactions. Their simulations were able to accurately predict the LOL at different ambient temperature conditions. Using a similar approach Vishwanathan and Reitz [14] captured the LOL and soot distribution under LTC conditions. Recently, Som and Aggarwal [4] developed an improved primary breakup model (KH-ACT) accounting for cavitation and turbulence-induced breakup in addition to aerodynamic breakup [4,15]. The KH-ACT model was coupled with a reduced NHPT model [16] to successfully predict the ignition and flame lift-off behavior for different injection and ambient conditions. Lucchini et al. [17] reported the relevance of a perfectly stirred reactor combustion model by showing that the mixture fraction variance is close to zero, hence, concluding that the turbulence-chemistry interactions may be neglected for modeling purposes. OpenFOAM was used with a 44 species, 112 reactions NHPT mechanism to predict ignition delay and LOL at different ambient temperatures and oxygen concentrations.

The influence of turbulence-chemistry interaction on spray combustion was accounted for by Azimov et al. [18] by using the ECFM3Z model. The model was able to accurately predict the influence of oxygen concentration on LOL. Tap and Veynante [19] used a combination of mixing, flame surface density, progress variable, and chemistry models to predict the ignition and flame stabilization phenomenon. Karrholm et al. [20] implemented a PaSR model for turbulence chemistry interactions in KIVA-3V and OpenFOAM codes. An NHPT reaction mechanism consisting of 83 species and 338 reactions was used to predict LOL and ignition delays. They attributed the differences in the prediction by the two codes to differences in computational mesh, sub-model implementation, and solution algorithms. Golovitchev et al. [21] also used the PaSR approach along with a 57 species, 217 reactions NHPT mechanism to predict soot distributions. An excellent review about the different approaches for modeling flame lift-off and stabilization has been performed by Venugopal and Abraham [22].

Accurate prediction of ignition delay and LOL depends heavily on the reaction mechanisms. Although the role of different combustion models and turbulence-chemistry interactions on spray combustion processes have been studied, as summarized above, the influence of chemical kinetic models on those processes has not been fully characterized. In addition, all of the above modeling approaches were based on the RANS approach. While Smagorinsky and dynamic structure LES models have been used emissions under LTC regimes [23], their ability to predict LOLs and ignition delays in constant volume combustion vessels has not been adequately assessed. Since diesel spray combustion processes are mixing controlled, improvements in predicting LOLs and ignition delays may be achieved with a LES model. This potential is the basis for the present numerical study, the primary objectives of which are to (1) compare ignition delays and LOLs predicted by different diesel and biodiesel surrogate mechanisms with the experimental data from Sandia and (2) compare the RANS and LES approaches under both non-reacting and reacting conditions for qualitatively and quantitatively predicting the spray and flame structures. Another objective of this study is to assess the computational efficiency and scalability of the detailed reaction mechanisms for diesel and biodiesel surrogates and to understand the computational costs associated with running these large mechanisms.

2 PHYSICAL-COMPUTATIONAL MODEL

Fuel spray and combustion simulations were performed using the Eulerian-Lagrangian approach in the computational fluid dynamics software CONVERGE [4,24,25]. It incorporates state-of-the-art models for spray injection, atomization and breakup, turbulence, droplet collision, and coalescence. The gas-phase flow field is described by using either the Favre-Averaged Navier-Stokes equations in conjunction with the RNG k-ε or the LES based turbulence model, which includes source terms for the effects of dispersed phase on gas-phase turbulence. These equations are solved by using a finite volume solver. The details of these models can be found in previous publications [26], so only a brief description is provided here.

Copyright © 2011 by ASME

The Kelvin-Helmholtz (KH) and Rayleigh-Taylor (RT) models are used to predict the subsequent secondary droplet breakup [27,28]. Droplet collisions are modeled with no time counter algorithm [29]. Once a collision occurs, the outcomes of the collision are predicted as bouncing, stretching, reflexive separation, or coalescence [30]. A droplet evaporation model based on the Frossling correlation is used. Also used is a dynamic drag model based on the postulation that the drag coefficient depends on the shape of the droplet, which can vary between a sphere and a disk. The effects of turbulence on the droplet are accounted for using a turbulent dispersion model. Detailed kinetic modeling is performed using the SAGE chemical kinetic solver [12,24,25] directly coupled with the gas-phase calculations using a well-stirred reactor model.

CONVERGE uses an innovative, modified cut-cell Cartesian method for grid generation [24,25]. The grid is generated internally at runtime. For all cases, the base grid size is fixed at 4 mm. In order to resolve the flow near the injector, a fixed grid embedding is employed such that the minimum grid size is 0.25 mm. Apart from this region, it is rather difficult to determine *a priori* where a refined grid is needed. Hence, four levels of adaptive mesh refinement are employed for the velocity field. To match the combustion chamber geometry used in the experimental study [11], a cubical geometry of 108 mm on each side is generated (cf. Fig. 1). The zoomed-in view of the fixed embedding region is also shown.

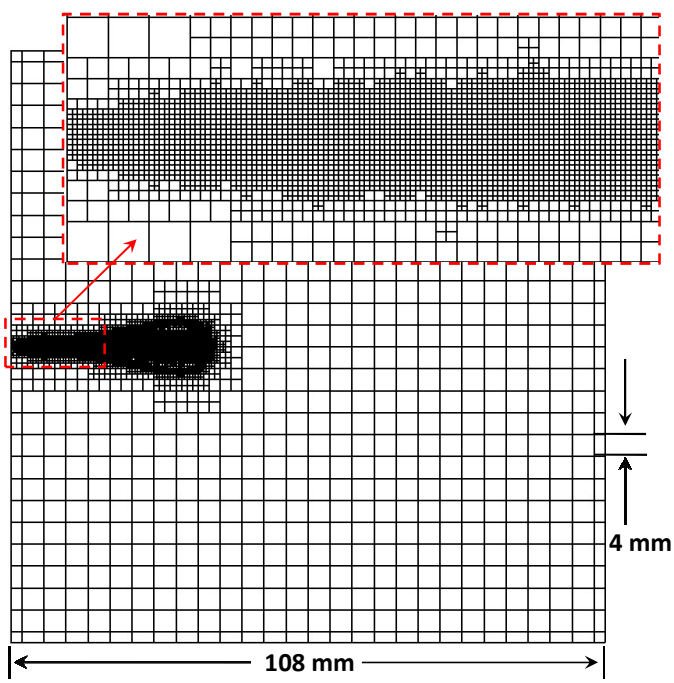

Figure 1: Grid generated in CONVERGE at 0.4 ms ASI for combusting sprays described in Table 1. The field of view is 108 mm each side.

<u>LES – Smagorinsky Based Turbulence Model</u>

Velocity and other thermodynamic variables are expressed in Favre form, whereas density and pressure are expressed in Reynolds form. The density-weighted LES spatial-filtering operation on the Navier-Stokes equation results in the filtered momentum equation:

$$\frac{\partial \bar{\rho}\tilde{u}_i}{\partial t} + \frac{\partial \bar{\rho}\tilde{u}_i\tilde{u}_j}{\partial x_j} = -\frac{\partial \bar{P}}{\partial x_i} - \frac{\partial \bar{\rho}T_{ij}}{\partial x_j} + \frac{\partial}{\partial x_j}\left(\mu\frac{\partial \tilde{u}_i}{\partial x_j}\right) - \bar{F}_i \quad (1)$$

where the LES sub-grid scale tensor:

$$T_{ij} = \left(\tilde{u}_i\tilde{u}_j - \tilde{u}_i\tilde{u}_j\right) \quad (2)$$

is modeled using a Smagorinsky-based model:

$$T_{ij} = -2C_s\Delta^2\left|\bar{S}\right|\bar{S}_{ij} + \frac{1}{3}\delta_{ij}T_{kk} \quad (3)$$

where $\left|\bar{S}\right| = \sqrt{2\bar{S}_{ij}\bar{S}_{ij}}$, $\Delta = V_{cell}^{1/3}$ (4)

and $\bar{S}_{ij} = \frac{1}{2}\left(\frac{\partial \bar{u}_i}{\partial x_j} + \frac{\partial \bar{u}_j}{\partial x_i}\right)$

The spray models require a turbulent kinetic energy for closure. For the Smagorinsky model, the sub-grid turbulent kinetic energy is not readily available. Hence, the following expression is used for closure:

$$k \cong C_{les}\frac{\Delta^2}{24}\frac{\partial \bar{u}_i}{\partial x_j}\frac{\partial \bar{u}_i}{\partial x_j} \quad (5)$$

The multi-component evaporation model implemented in CONVERGE is based on a discrete approach. This model is used to simulate a three-component biodiesel mixture as discussed in the next section. For this model, the liquid drops are assumed to be perfectly mixed. The liquid and gas properties for each specie component are considered in the calculations. The vapor pressure calculations (critical for accurate evaporation) are performed by using Raoult's Law.

3 Results and Discussion

This section is divided into three parts. The first part discusses the influence of reduced chemical kinetic mechanisms for NHPT and biodiesel on ignition delay and flame lift-off characteristics. Next the influence of RANS and LES turbulence models on spray and flame structure is analyzed. The last section deals with the scalability and - computational efficiency of the chemical kinetic mechanisms discussed in the context of section 3.1.

3.1 Comparison of Chemical Kinetic Mechanisms for Diesel and Biodiesel

First we present validation for NHPT as a diesel surrogate. The data was obtained from Sandia National Laboratories [11]. A parametric study was performed to capture the influence of

Copyright © 2011 by ASME

ambient temperature on LOL and ignition delay. The conditions simulated are mentioned in Table 1. It should be noted that simulations were first performed under non-reacting conditions (absence of O_2) to ensure that spray penetration, liquid length, and vapor penetration (not shown here) are accurately predicted by the spray models under evaporating conditions. In order to capture the influence of reaction mechanisms on flame LOLs and ignition delays, two NHPT mechanisms from the literature are chosen. The first mechanism was developed at Chalmers University [16] and consists of 42 species and 168 reactions. The second mechanism was developed recently by Lu et al. [31] and consists of 68 species and 283 reactions. Both mechanisms consist of the low-temperature chemistry and can capture the NTC behavior. All of the simulations in this section were performed with the RNG k-ε turbulence model.

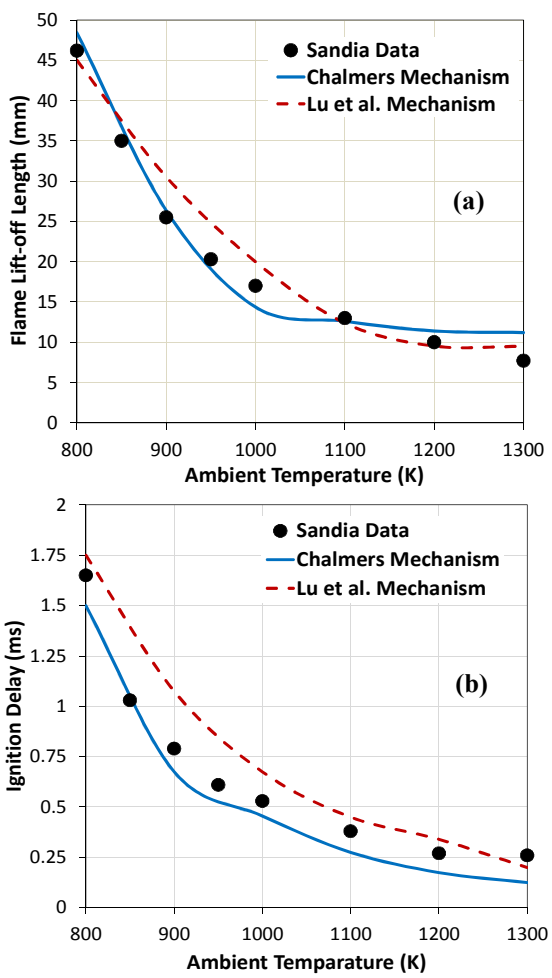

Figure 2: Measured [11] (a) flame LOL and (b) ignition delay vs. ambient temperature calculated by using Chalmers and Lu et al. mechanisms, respectively, for NHPT.

Figure 2 presents a comparison of the measured [11] and predicted flame LOLs and ignition delays as a function of ambient temperature, calculated using the two NHPT mechanisms described above. In simulations, flame LOL is determined by the nearest location of OH radical contour corresponding to Y_{OH} = 0.05% of the peak value, from the point of injection. An increase in ambient temperature (keeping ambient density constant) results in lowered flame LOL due to the increased chemical reactivity, which moves the ignition and flame stabilization locations upstream. Increased ambient temperatures also results in decreased ignition delays as expected. In general, both mechanisms predict the overall trends of LOLs and ignition delays very well, while the Lu et al. mechanism always predicts higher ignition delays compared to the Chalmers mechanism. Ignition delay in a two-phase flow consists of physical and chemical delays. Since the spray structure, i.e., SMD, spray penetration etc. (not shown here), is similarly predicted with both mechanisms, the differences in the predicted ignition delays should be primarily attributable to the differences in the chemical kinetic mechanisms. It is also observed that the Lu et al. mechanism performs marginally better especially under low and high ambient temperature conditions.

Fuels	NHPT, Diesel # 2
Ambient Temperature (K)	800-1300: Parametric study
Ambient Density (kg/m^3)	14.8
Composition	Reacting: 21% O_2
Injection pressure (bar)	1500
Fuel injection temperature (K)	373
Fuel Density at 300K (kg/m^3)	NHPT: 700 Diesel # 2: 820
Nozzle diameter (μm)	100
Duration of Injection (ms)	5
Discharge Coefficient	0.75-0.80

Table 1: Range of conditions for the combusting spray experiments at Sandia National Laboratories [11].

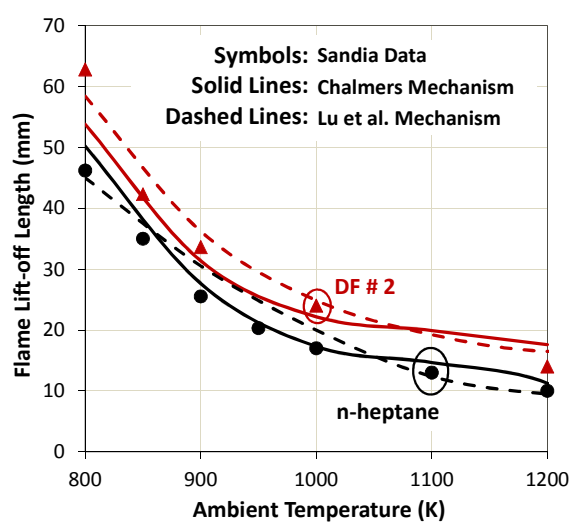

Figure 3: Measured [11] and predicted flame LOL vs. ambient temperature for NHPT and DF # 2, calculated using Chalmers and Lu et al. mechanisms, respectively.

Copyright © 2011 by ASME

Since both the Chalmers and Lu et al. mechanisms performed well in predicting the LOLs and ignition delays for NHPT, these mechanisms were used to predict the LOL characteristics of diesel # 2 (DF # 2). Note that the physical properties of n-tetradecane were used to represent DF # 2. Figure 3 presents the effect of ambient temperature on LOL for DF # 2 and NHPT. The data for NHPT and DF # 2 are at different injection conditions hence, it is not appropriate to compare the LOL characteristics between these fuels from Fig. 3. In general, both mechanisms are able to predict the LOL trends very well. However, Lu et al. mechanism does a marginally better job in predicting the flame LOLs of DF # 2.

The influence of chemical kinetic mechanisms on the spray, LOL, and ignition characteristics of different biodiesel surrogates will be further explored in this section. The experimental data was obtained by Pickett et al. [32]. Three different mechanisms will be investigated. Recently, two reduced mechanisms with a mixture of MD (25%), MD9D (25%), and NHPT (50%) were developed at the University of Connecticut [33]. The detailed mechanism was obtained from Lawrence Livermore National Laboratory, consisting of 3299 species and 10806 elementary reactions [34]. The first reduced mechanism consists of 123 species and 394 reactions (designated as UConn-123) and was obtained with a worst-case error tolerance of 40% for auto-ignition delays and extinction residence times in perfectly stirred reactors [33]. This is perhaps the largest mechanism employed so far for spray combustion simulations with the grid size of interest (0.25 mm). The second reduced mechanism consists of 89 species and 364 reactions (designated as UConn-89) and was obtained with a worst-case error tolerance of 30% [35]. In the past, a surrogate mixture of 33% methyl Butanoate (MB) and 67% NHPT [36], consisting of 41 species and 150 reactions (designated as ERC-bio) has also been used for biodiesel combustion modeling [37]. This surrogate model will also be tested against the above reaction mechanisms. Note that physical properties of biodiesel are represented by the properties of methyl oleate, and MD+MD9D+NHPT and MB+NHPT are only used as chemical kinetic surrogates for biodiesel.

Injection system	Bosch common rail
Nozzle description	Single-hole, mini-sac
Duration of Injection [ms]	7.5
Orifice Diameter [μm]	90
Injection Pressure [bar]	1500
Fill Gas Composition (mole fraction)	Non-reacting: O_2=0% Reacting: O_2=15%
Chamber Density [kg/m^3]	22.8
Chamber Temperature [K]	900, 1000
Fuel Density at 300 K [kg/m^3]	877

Table 2: Test conditions for biodiesel combustion experiments at Sandia [11].

Validation under non-reacting conditions will be presented first, followed by reacting conditions. Figure 4 presents predicted and measured liquid spray and fuel vapor penetration at different times ASI under non-reacting conditions. The experimental conditions are listed in Table 2. An increase in ambient temperature from 900 K to 1000 K at fixed ambient density causes a decrease in spray penetration, which is due to the increased vaporization rate, and, subsequently, decreased liquid length. Simulations are able to capture the spray penetration characteristics very well at both ambient-temperature conditions. Similarly, fuel vapor penetration is also well predicted by the simulations at an ambient temperature of 900 K. It is noted that in simulations the vapor penetration at any time is determined from the farthest downstream location of 0.05 fuel mass-fraction contour.

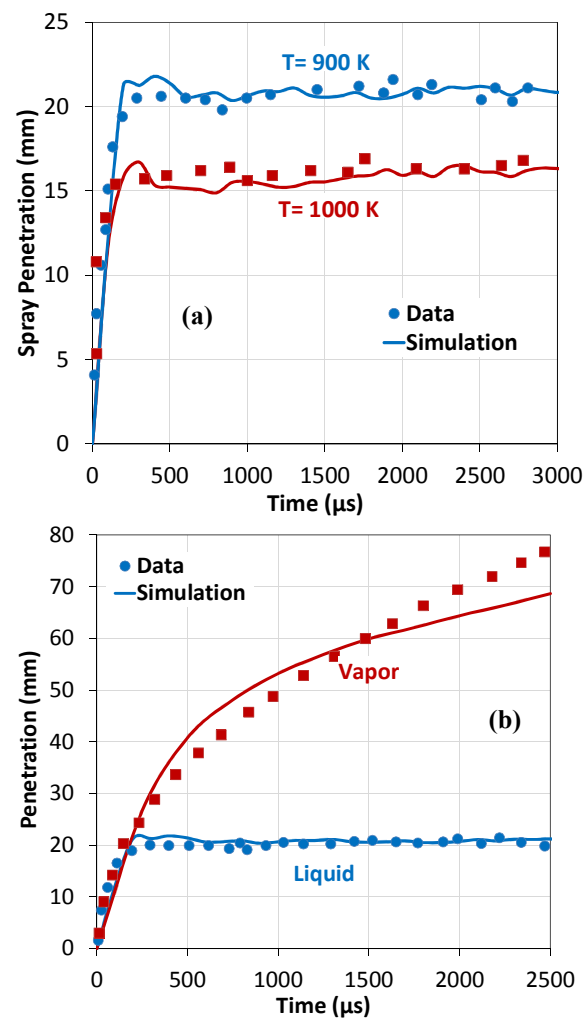

Figure 4: Measured [11] and predicted (a) spray penetration vs. time and (b) vapor penetration vs. time, under non-reacting conditions at an ambient temperature of 900 K for biodiesel fuel.

Copyright © 2011 by ASME

Figure 5 presents measured [11] and computed OH profiles under conditions presented in Table 2 at a chamber temperature of 1000 K. Because of the axisymmetric nature of the spray and combustion processes, images are presented on a cut-plane through the center of the fuel jet. The LOL is shown by a vertical white-dashed line, and the average equivalence ratio at the lift-off location is also shown for all of the mechanisms. The spray axis is demarcated by using a horizontal white-dashed line. The field of view is 75 mm × 25 mm in the axial and transverse directions, respectively. The LOL is over-predicted by about 25% and 50% with UConn-123 and UConn-89 mechanisms, respectively. The width of the flame is well captured by all of the mechanisms. The measured ignition delay is 396 µs (cf. Table 3), while the simulated values are 510 µs and 580 µs with UConn-123 and UConn-89 mechanisms, respectively. On the other hand, the ERC-bio mechanism underpredicts LOL by about 50%, and the predicted ignition delay is 220 µs. In simulations, ignition is said to occur when temperatures are higher than 2000 K around the periphery of the jet. It is well known that LOL and ignition delay are correlated [38], which is also observed in the present simulations.

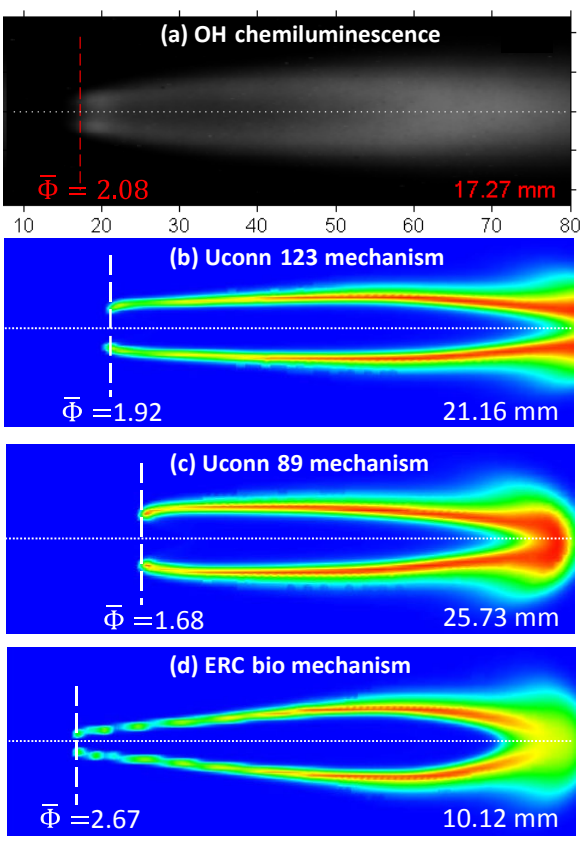

Figure 5: Flame LOL predicted by the three mechanisms compared with the OH-chemiluminescence data from Sandia [11]. The average equivalence ratio at flame lift-off location is also indicated.

Figure 5 also compares the average equivalence ratio at the flame lift-off location between experiments and predictions. Pickett et al. [6,7] showed that if the equivalence ratio at LOL is less than 2, the total soot production can be reduced or even inhibited. Thus the average equivalence ratio at LOL not only provides information about local mixing but also is indicative of the sooting tendency of the flame. Hence, it is important to predict this value accurately. In experiments once the LOL is measured, the average equivalence ratio is determined by averaging the equivalence ratio across a transverse line at the lift-off location (white dashed line) across the width of the flame, as proposed by Siebers and co-workers [1,6,7,10]. The mechanism that predicts the highest LOL is seen to predict the lowest average equivalence ratio which is expected. The ERC-bio mechanism is seen to grossly overpredict the average equivalence ratio value at the lift-off location.

The liquid length and spray penetration matched well (cf. Fig. 4) with the experimental data, thereby showing the model's capability to predict the mixing process. Hence, the over-prediction of flame LOL and ignition delay and the under prediction of average equivalence ratio for UConn-123 and UConn-89 mechanisms could be due to either the uncertainties in the detailed mechanism or the reduction errors in the skeletal mechanism. Since the MB molecule is a saturated molecule with only 5 carbon atoms, it is perhaps not an ideal surrogate for long-chained unsaturated biodiesel fuels. This may be the main reason for the predicted trends with this mechanism. Under the conditions investigated, the UConn-123 mechanism seems to be most accurate in predicting ignition delays and flame LOLs.

	Ignition Delay [µs]
Sandia Data [32]	396
UConn-123 mechanism	510
UConn-89 mechanism	580
ERC-bio mechanism	220

Table 3: Measured [11] and predicted ignition delay using the three biodiesel surrogate mechanisms discussed in context of Fig. 5.

Figure 6 plots the measured [11] and predicted spray penetration with UConn-123 species and ERC-bio mechanisms, respectively, as a function of time under reacting conditions described in the context of Fig. 5. The spray penetration and liquid length are substantially underpredicted by the ERC-bio mechanism. This is surprising since the only difference between these simulations is the choice of reaction mechanisms and the accompanying thermodynamic data. The reason for these differences in spray penetration is further analyzed in Fig. 7.

Figure 7 plots the computed temperature profiles at different times ASI under conditions discussed in Fig. 6, using UConn-123 and ERC-bio mechanisms, respectively. Due to the axisymmetric nature of the flow field, images are presented on a cut-plane through the center of the fuel jet. The flame LOL and

Copyright © 2011 by ASME

liquid length are marked by white solid and dashed lines respectively. The spray axis is also demarcated, along with the ignition kernels and liquid spray location. The field of view is 108 mm x 40 mm in the axial and transverse directions respectively. A zoomed view of the flame structure at 3000 µs is also shown.

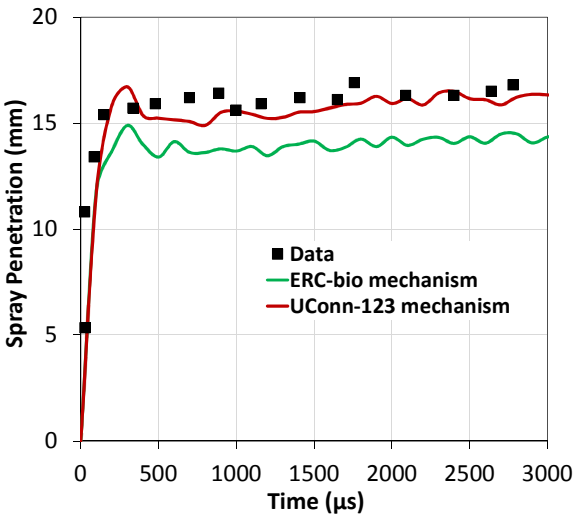

Figure 6: Measured [11] and predicted spray penetration, with UConn-123 and ERC-bio mechanisms, respectively, as a function of time at an ambient temperature of 1000 K under reacting conditions.

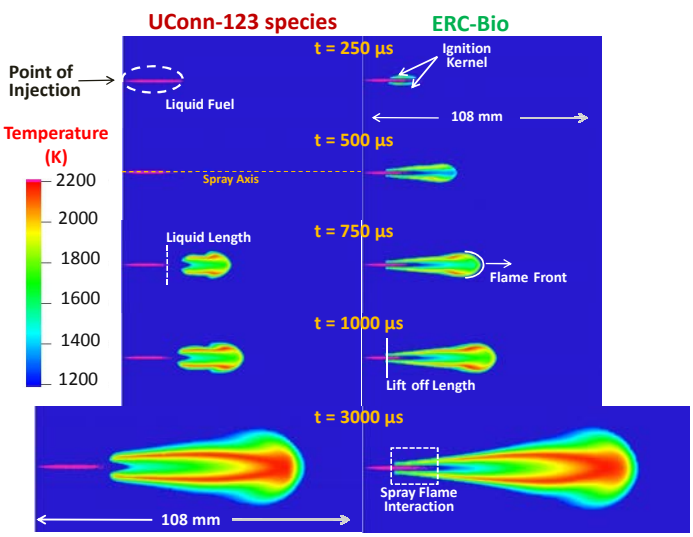

Figure 7: Computed liquid fuel penetration and temperature contours predicted by using UConn-123 and ERC-bio mechanisms, respectively, for the spray flames plotted in Fig. 6.

The difference in flame structure predicted by these mechanisms is very apparent. Ignition occurs earlier with the ERC-bio mechanism as seen by the ignition kernels at 250 µs. At 500 µs, a fully developed flame is observed with the ERC-bio mechanism, while the UConn-123 mechanism is yet to ignite. Consequently, at 750 µs and 1000 µs, higher flame lengths were predicted with the ERC-bio mechanism. Another interesting point to note is that for the ERC-bio mechanism, AN ignition kernel is established in the liquid spray region. This implies that there is significant spray-flame interaction (also seen at 3000 µs) with this mechanism. The hot flame enveloping the cold spray enhances the evaporation rate, thus decreasing the spray penetration and liquid length as a result of using the ERC-bio mechanism.

3.2 Comparison of RANS vs. LES Modeling Approaches

In this section, standard RANS based approach are compared against a high-fidelity LES based approach under non-reacting and reacting conditions against both quantitative and qualitative data from Sandia [11]. The standard modeling approach consists of using a coarser minimum grid size with RANS based models (similar to studies reported in literature [4,12-14,17-22,37]), whereas, the high-fidelity approach consists of using a finer mesh (such as 0.125mm) with LES models. Smaller grid sizes were necessary with the LES model for two reasons: (1) since a zero-equation Smagorinsky model is being used, it is desirable that the sub-grid scale modeling is reduced, and (2) the possibility of accurately capturing the large-scale flow structures is higher with a finer grid. The comparisons under non-reacting conditions are presented first.

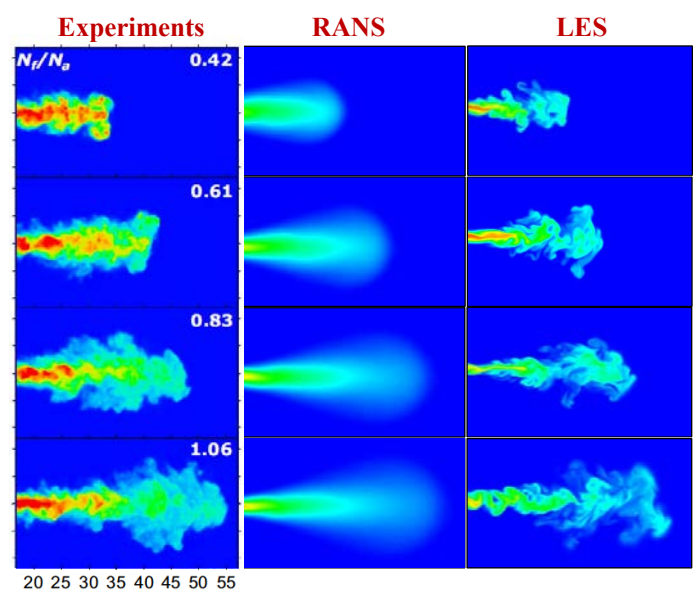

Figure 8: Images comparing the equivalence ratio calculated using RANS and LES models, respectively, against the experimental data from Sandia [11] under non-reacting conditions.

The conditions of the non-reacting experiments are shown in Table 1, with the ambient temperature being 1000K. The instantaneous experimental images obtained using Rayleigh scattering imaging are shown on the left along with the time ASI

Copyright © 2011 by ASME

and the axial length scale. The field of view is 40 mm x 20 mm in the axial and transverse directions respectively. Note that the experimental contours pertain to a ratio between fuel-air number densities (N_f/N_a) whereas; simulations plot the fuel mass-fractions. Fuel vapor penetration and dispersion can be clearly seen from the experimental and simulation plots. Both RANS and LES simulations predict the dispersion and vapor penetration fairly well. However, marked differences in the spray structure are clearly observed between RANS and LES cases. While RANS predicts smooth, averaged profiles, the LES simulation is able to capture the instantaneous structure well. However, the initiation of instabilities on the surface seems to be occurring further downstream in the case of LES compared to the experiments. Spray dispersion seems to be marginally underpredicted by the LES model as well. Early initiation of instabilities results in an early jet breakup which can enhance the spray and vapor dispersion as well.

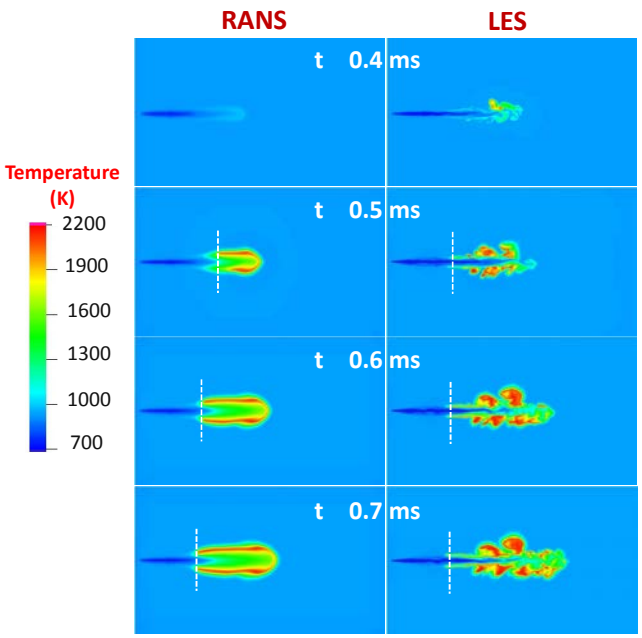

Figure 9: Comparison of predicted temperature contours calculated using RANS (RNG k-ε) and LES (Smagorinsky) turbulence models, respectively, at different times ASI.

With the qualitative validation under non-reacting conditions, RANS and LES models are now compared under reacting conditions for NHPT. The test conditions simulated are shown in Table 1. Figure 9 presents the evolution of temperature contours with RANS and LES modeling approaches at an initial ambient temperature of 1000K. The white dashed line demarcates the predicted LOL at that time. There are several interesting differences between the simulations:

(1) Ignition seems to occur earlier for the LES model with temperatures higher than 2000 K at 0.4ms. This is expected due to enhanced flow structure with the LES model.

(2) - The temperature contours are smooth with the RANS model which is expected since it predicts a time-averaged mean value for the temporal variation. On the other hand, LES based on filtering rather than averaging can capture the temporal fluctuations of the same scale as the minimum grid size or higher.

(3) - Volumetric auto-ignition is observed with the LES model, and the flame seems to be stabilized as a result of the spontaneous ignition phenomenon. However, with RANS the flame seems to be propagating upstream before being stabilized. This is also shown with the change in LOL at different times ASI. The RANS model shows that the LOL decreases with time; but the LES predicts only a minor change in LOL. Pickett et al. [39] have shown that flame stabilization seems to occur as a result of successive auto-ignition of the incoming fuel at the flame lift-off location rather than by flame propagation upstream. Hence, the results from the LES model clearly are more representative of the actual spray combustion process.

(4) - Quasi-steady LOL values predicted by both models are very similar.

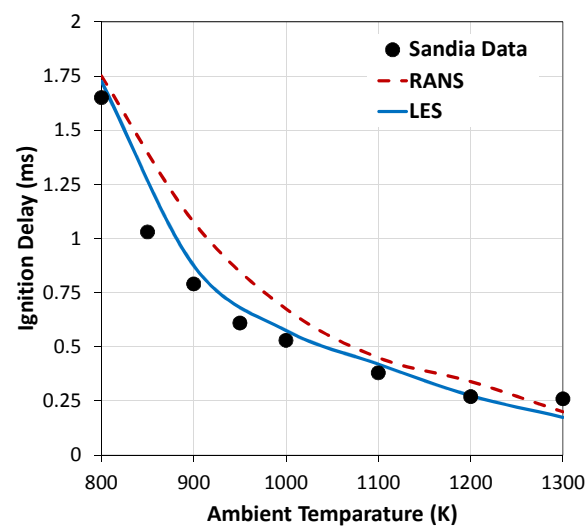

Figure 10: Measured [11] and predicted ignition delay vs. ambient temperature for NHPT calculated by using RANS and LES turbulence models, respectively.

In Fig. 10, quantitative comparisons of predicted ignition delays at different ambient temperatures by RANS and LES turbulence models are presented. The data for NHPT were obtained at Sandia [11]. The Lu et al. mechanism for NHPT was used for predicting ignition delays for both turbulence models. It is clear that the LES model predicts lower ignition delay values which is perhaps because of the enhanced flow structures. Also, under the conditions investigated it seems that the LES model performs marginally better than the RANS model in predicting ignition delays at different ambient temperatures. Flame LOL validation is not presented since the quasi-steady LOL value predicted by the RANS and LES

Copyright © 2011 by ASME

models were close and both agree very well with the experimental data.

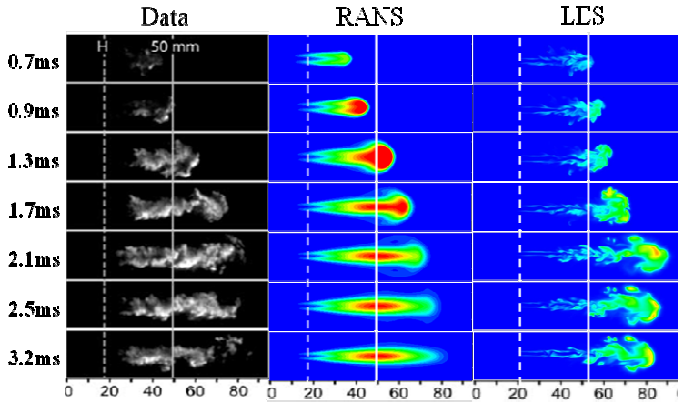

Figure 11: Time sequence of PLII images and predicted soot mass fraction contours [6,7] by using RANS and LES models, respectively.

Planar laser-induced incandescence (PLII) images of soot [6,7] along a thin plane of the fuel jet were compared with model predictions by RANS and LES in Fig. 11. Time ASI for each image is shown on the left thus the temporal evolution of a typical combustion event is seen. Distance from the injector is shown at the bottom while the dashed and solid vertical lines represent LOL (19mm) and an axial position of 50mm respectively. The soot mass production within a computation cell is determined from a single-step competition between formation and oxidation rates of C_2H_2 species, based on the Hiroyasu model [40]. This soot model has been extensively used in the literature. It can be seen that the predicted soot distributions agree well with the experimental results. The experimentally observed trend that soot generation occurs beyond the LOL is also well captured by both RANS and LES models. The instantaneous structure of soot though is better captured by the LES model. The RANS model on the other hand provides an averaged soot distribution contour.

3.3 Computational Scalability and Efficiency Analysis

The last section examines computational efficiency and scalability of the different reaction mechanisms discussed in section 3.1. All the simulations were performed on the FUSION cluster at Argonne National Laboratory. This cluster has 320 compute nodes each with 2.6 GHz Pentium Xeon CPUs and 36GB of RAM. Each node is a dual-socket, quad-core (8 processors per node) resulting in a total of 2560 processors. The computational time to run the large biodiesel mechanisms on a single node is shown in Table 4. Doubling the size of the mechanism from 41 species (ERC-bio) to 89 species (UConn-89) increases the computational time by three times, whereas tripling to 123 species (UConn-123) results in an increase in computational time of about 6 times.

Mechanisms	Computational time (one node)
UConn-123	74 hours
UConn-89	38 hours
ERC-bio	13 hours

Table 4: Run-times for ERC-bio, UConn-89, and Uconn-123 mechanisms on one node.

The computational efficiency and scalability per node plotted in Fig. 12 are defined below:

$$\text{Scalability per node} = \frac{T_1}{T_n} \tag{6}$$

$$\text{Efficiency per node} = \frac{T_1 \times 100}{nT_n} \tag{7}$$

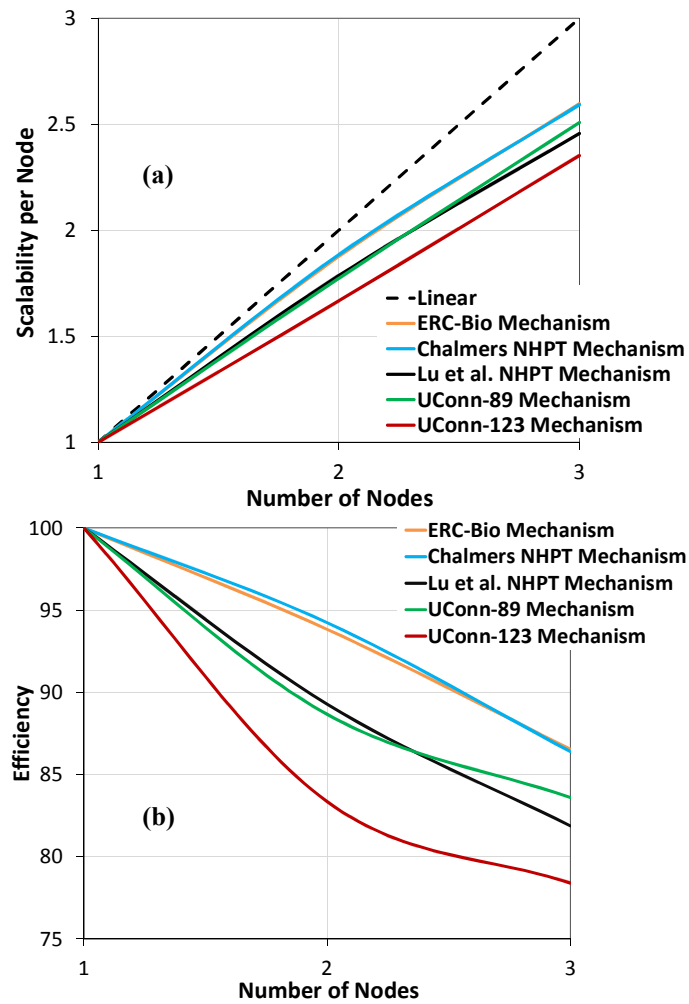

Figure 12: (a) Scalability and (b) computational efficiency per node for the diesel and biodiesel surrogate mechanisms discussed in the context of section 3.1.

Linear scalability is shown with the black dashed line in Fig. 12a. It is clearly seen that as the size of the mechanism increases (in terms of species), the scalability per node

Copyright © 2011 by ASME

decreases. Hence, ERC-bio and Chalmers NHPT mechanisms which consist of 41 and 42 species respectively predict the best scalability whereas; the UConn-123 mechanism predicts the worst scalability. Due to the reduced scalability with the larger mechanisms, it is not surprising that the computation efficiency is also lower. Consequently, ERC-bio mechanism predicts the highest computational efficiency amongst the investigated mechanisms. Since the UConn-123 mechanism did the best job in predicting experimental trends, it is obvious that the higher fidelity results are associated with greater computational cost.

4 Conclusions

This study focused on evaluating the use of realistic chemical kinetic models for diesel and biodiesel surrogate fuels, and the Smagorinsky-based LES turbulence model. The following conclusions can be drawn:

1) While both Lu et al. and Chalmers mechanisms can well predict the LOL and ignition delay characteristics of NHPT fuel, the Lu et al. mechanism predicts these parameters marginally better for DF # 2.
2) The UConn-123 mechanism does the best job in predicting biodiesel ignition delays and LOLs. This is not surprising since the mixture of MD+MD9D+NHPT is a more realistic surrogate for biodiesel.
3) The Smagorinsky based LES model captures the instantaneous soot contours under reacting conditions, equivalence ratio contours under non-reacting conditions, better than the RANS simulations.
4) The LES model also predicts volumetric auto-ignition and a fairly stabilized LOL, which is more realistic in these conditions. In contrast, the RANS model predicts ignition kernels moving upstream, which is inconsistent with the experimental results from Sandia.
5) Smaller mechanisms result in higher scalability and greater computational efficiency at the cost of compromised accuracy in the present simulations, while larger and more predictive mechanisms, especially for biodiesel, are more expensive.

ACKNOWLEDGMENTS

The submitted manuscript has been created by UChicago Argonne, LLC, operator of Argonne National Laboratory (Argonne). Argonne, a U.S. Department of Energy Office of Science laboratory, is operated under Contract No. DE-AC02-06CH11357. The U.S. Government retains for itself, and others acting on its behalf, a paid-up, nonexclusive, irrevocable worldwide license in said article to reproduce, prepare derivative works, distribute copies to the public, and perform publicly and display publicly, by or on behalf of the Government.

The work at University of Connecticut was supported by the National Science Foundation under Grant 0904771. Any opinions, - findings, and conclusions or recommendations expressed in this material are those of the authors and do not necessarily reflect the views of the National Science Foundation.

The authors gratefully acknowledge a grant of computing resources -at the Laboratory Computing Resource Center at Argonne National Laboratory.

The authors gratefully acknowledge Dr. Lyle Pickett from Sandia National Laboratory for sharing diesel, n-heptane, and biodiesel data.

NOMENCLATURE

C_s	Smagorinsky model constant (= 0.2) -
C_{les}	LES Model constant (= 2.0) -
F_i	Source term due to drag on droplets [Pa] -
P	Pressure of gas mixture [Pa] -
S_{ij}	Symmetric stress tensor [m^2/s^2] -
T_i	Time taken to complete a simulation with i nodes [s] -
T_{ij}	LES sub-grid scale tensor [m^2/s^2] -
V_{cell}	Cell volume [m^3] -
n	Number of compute nodes -
t	Time [s] -
u	Gas velocity [m/s] -
Δ	Filter size [m] -
δ	Kronecker delta -
k	Sub-grid scale turbulent kinetic energy [m^2/s^2] -
μ	Dynamic Viscosity [Pa.s] -
ρ	Density of the gas mixture [kg/m^3] -

ABBREVIATION

ASI -	After start of injection
CI -	Compression ignition
ID -	Ignition delay
KH-ACT -	Kelvin-Helmholtz aerodynamics cavitation turbulence induced primary breakup model
LES -	Large eddy simulation
LOL -	Lift-off length
LTC -	Low-temperature combustion
MB -	Methyl butanoate
MD -	Methyl decanoate
MD9D -	Methyl 9-decanoate
NHPT -	n-heptane
NTC -	Negative temperature coefficient
PaSR -	Partially stirred reactor
PLII -	Planar laser-induced incandescence
RANS -	Reynolds-averaged Navier-Stokes
SMD -	Sauter-mean diameter

REFERENCE

1. - Naber, J.D., Siebers, D.L., 1996, “Effects of gas density and vaporization on penetration and dispersion of diesel sprays”, SAE Paper No. 960034.

 Copyright © 2011 by ASME

2. - Higgins, B.S., Siebers, D.E., 2001, “Measurement of the Flame Lift-off Location on DI Diesel Sprays Using OH Chemiluminescence”, SAE Paper No. 2001-01-0918.
3. - Siebers, D.L., Higgins, B.S., “Flame Lift-off on Direct-Injection Diesel Sprays under Quiescent Conditions”, SAE Paper No. 2001-01-0530.
4. - Som, S., Aggarwal, S.K., 2010, “Effects of primary breakup modeling on spray and combustion characteristics of compression ignition engines”, Combustion and Flame, Vol. 157, pp.1179-1193.
5. - Siebers, D.L., 1998, “Liquid-phase fuel penetration in diesel sprays”, SAE Paper No. 980809.
6. - Pickett, L.M., Siebers, D.L., 2004, “Soot in diesel fuel jets: effects of ambient temperature, ambient density, and injection pressure”, Combustion and Flame, Vol. 138, pp. 114-135.
7. - Pickett, L.M., Siebers, D.L., 2002, “An investigation of diesel soot formation processes using micro-orifices”, Proceedings of the Combustion Institute, Vol. 29, pp. 655-662.
8. - Idicheria, C.A., Pickett, L.M., 2007, “Effect of EGR on diesel premixed-burn equivalence ratio”, Proceedings of the Combustion Institute, Vol. 31, pp. 2931-2938.
9. - Idicheria, C.A., Pickett, L.M., 2007, “Quantitative mixing measurements in a vaporizing diesel spray by Rayleigh imaging”, SAE Paper No. 2007-01-0647.
10. -Pickett, L.M., Manin, J., Genzale, C.L., Siebers, D.L., Musculus, M.P.B., Idicheria, C.A., 2011, “Relationship between diesel fuel spray vapor penetration/dispersion and local fuel mixture fraction”, SAE Paper No. 2011-01-0686.
11. -http://www.sandia.gov/ecn/
12. -Senecal, P.K., Pomraning, E., Richards, K.J., 2003, “Multi-Dimensional Modeling of Direct-Injection Diesel Spray Liquid Length and Flame Lift-off Length using CFD and Parallel Detailed Chemistry”, SAE Paper No. 2003-01-1043.
13. -Kong, S.C., Sun, Y., Reitz, R.D., 2007, “Modeling Diesel Spray Flame Lift-off, Sooting Tendency, and NOx Emissions Using Detailed Chemistry with Phenomenological Soot Model”, Journal of Gas Turbine and Power, Vol. 129, pp. 245-251.
14. -Vishwanathan, G., Reitz, R.D., 2008, “Numerical predictions of diesel flame lift-off length and soot distributions under low temperature combustion conditions”, SAE Paper No. 2008-01-1331.
15. -Som, S., Ramirez, A.I., Aggarwal, S.K., Kastengren, A.L., El-Hannouny, E.M., Longman, D.E., Powell, C.F., Senecal, P.K., 2009, “Development and Validation of a Primary Breakup Model for Diesel Engine Applications”, SAE Paper No. 2009-01-0838.
16. -http://www.tfd.chalmers.se/~valeri/MECH.html
17. -Lucchini, T., D’Errico, G.D., Ettore, D., Ferrari, G., 2009, “Numerical investigation of non-reacting and reacting diesel sprays in constant-volume vessels”, SAE Paper No. 2009-01-1971.
18. -Azimov, U., Kawahara, N., Tomita, E., Tsuiboi, K., 2010, “Evaluation of the flame lift-off length in diesel spray combustion based on flame extinction”, Journal of Thermal Science and Technology, Vol. 5 (2), pp. 238-251.
19. -Tap, F.A., Veynante, D., 2005, “Simulation of flame lift-off on a diesel jet using a generalized flame surface density modeling approach”, Proceedings of the Combustion Institute, Vol. 30, pp. 919-926.
20. -Karrholm, F.P., Tao, F., Nordin, N., 2008, “Three-Dimensional Simulation of Diesel Spray Ignition and Flame Lift-off Using OpenFOAM and KIVA-3V CFD Codes”, SAE Paper No. 2008-01-0961.
21. -Golovitchev, V. I., Nordin, N., Jarnicki, R., Chomiak, J., 2000, "3-D Diesel Spray Simulations Using a New Detailed Chemistry Turbulent Combustion Model," SAE Paper No. 2000-01-1891.
22. -Venugopal, R., Abraham, J., 2007, “A numerical investigation of flame lift-off in diesel jets”, Combustion science and technology, Vol. 179, pp. 2599-2618.
23. -Banerjee, S., Rutland, C., 2011, “Numerical study of diesel combustion engines”, SAE Paper No. 2011-01-0823.
24. -Senecal, P.K., Richards, K.J., Pomraning, E., Yang, T., Dai, M.Z., McDavid, R.M., Patterson, M.A., Hou, S., Sethaji, T., 2007, “A new parallel cut-cell Cartesian CFD code for rapid grid generation applied to in-cylinder diesel engine simulations”, SAE Paper No. 2007-01-0159.
25. -Richards, K.J., Senecal, P.K., Pomraning, E., 2008, CONVERGE^{TM} (Version 1.2) Manual, Convergent Science, Inc., Middleton, WI.
26. -Som, S., 2009, “Development and Validation of Spray Models for Investigating Diesel Engine Combustion and Emissions;” PhD thesis, University of Illinois at Chicago.
27. -Reitz, R.D., 1987, “Modeling Atomization Processes in High Pressure Vaporizing Sprays”, Atomization and Spray Technology, Vol. 3, pp. 309-337.
28. -Patterson, M.A., Reitz, R.D., 1998, “Modeling the Effects of Fuel Spray Characteristics on Diesel Engine Combustion and Emissions”, SAE Paper No. 980131.
29. -Schmidt, D.P., Rutland, C.J., 2000, “A New Droplet Collision Algorithm”, Journal of Computational Physics, Vol. 164, pp. 62-80.
30. -Post, S.L., Abraham, J., 2002, “Modeling the outcome of drop-drop collisions in diesel sprays”, International Journal of Multiphase Flow, Vol. 28, pp. 997-1019.
31. -Lu, T. F., Law, C.K., Yoo, C.S., Chen J.H., 2009, "Dynamic Stiffness Removal for Direct Numerical Simulations", Combustion and Flame, Vol. 156 (8), pp.1542-1551.
32. -Nerva, J.G., Genzale, C.L. Oliver, J.M., Pickett, L.M., 2011, “Fundamental spray and combustion measurements of biodiesel under diesel steady conditions”, under preparation.

 Copyright © 2011 by ASME

33. -Luo, Z., Plomer, M., Lu, T., Som, S., Longman, D.E., 2011, “A reduced mechanism for biodiesel surrogates for low temperature chemistry”, 7th US Combustion Institute meeting, Paper No. 18.
34. -Herbinet, O., Pitz, W.J., Westbrook, C.K., 2010, “Detailed chemical kinetic oxidation mechanism for a biodiesel surrogate”, Combustion and Flame, Vol. 157, pp. 893-908.
35. -Som, S., Longman, D.E., Luo, Z., Plomer, M., Lu, T., 2011, “Modeling biodiesel spray flame lift-off and emission characteristics using a detailed mechanism for methyl decanoate as surrogate”, SAE 11PFL-0227.
36. -Brakora, J.L., Ra, Y., Reitz, R.D., McFarlane, J., Law, C.S., 2008, “Development and validation of a reduced reaction mechanism for biodiesel-fueled engine simulation” SAE Paper No. 2008-01-1378.
37. -Som, S., Longman, D.E., 2011, Numerical study comparing the combustion and emission characteristics of biodiesel to petrodiesel”, Energy and Fuel, Vol. 25, pp. 1373-1386.
38. -Pickett, L.M., Siebers, D.L., Idicheria, C.A., 2005, “Relationship between ignition processes and the lift-off length of diesel fuel jets”, SAE Paper No. 2005-01-3843.
39. -Pickett, L.M., Kook, S., Persson, H., Andersson, O., 2009, “Diesel fuel jet lift-off stabilization in the presence of laser-induced plasma ignition”, Proceedings of the Combustion Institute, Vol. 32, pp. 2793-2800.
40. -Heywood, J.B., 1998, “Internal Combustion Engine Fundamentals”. McGraw-Hill, Inc.

Copyright © 2011 by ASME